# Patterned surfaces with the controllable drug doses using inkjet printing

Sina Azizi Machekposhti[1*], Bin Zhang[1,2*], Roger Sachan[3], Lyndsi Vanderwal[4], Shane J. Stafslien[4], Roger J. Narayan[1†]

[1]Joint Department of Biomedical Engineering, University of North Carolina and North Carolina State University, Raleigh, North Carolina, USA
[2]Department of Mechanical Engineering, University College London, London, UK
[3]Department of Materials Science & Engineering, North Carolina State University, Raleigh, North Carolina, USA
[4] Department of Coatings & Polymeric Materials, North Dakota State University, 1715 NDSU Research Park Drive, Fargo, North Dakota 58102

[*]The first two authors contributed equally to this work.
[†]Corresponding author.
Roger Narayan
T 1 919 696 8488
F 1 509 696 8481
E rjnaraya@ncsu.edu

**Abstract**

A mixture of microflora, including *Staphylococcus aureus*, *Pseudomonas aeruginosa*, and *Candida albicans*, are found in burns and traumatic wounds. In this study, piezoelectric inkjet printing was used to apply an antifungal agent, amphotericin B, and an antibacterial agent, azithromycin, to the surfaces of gauze, silicon, and aluminum. The *in vitro* disk diffusion assay was performed on the unmodified, dimethyl sulfoxide vehicle-modified, azithromycin-modified, and amphotericin B-modified surfaces. Unlike the unmodified and dimethyl sulfoxide vehicle-modified surfaces, the amphotericin B-modified surfaces showed antifungal activity against *C. albicans*; the azithromycin-modified surfaces showed antibacterial activity against *Staphylococcus aureus* and *P. aeruginosa*. The dimethyl sulfoxide vehicle-modified surface did not show activity against *S. aureus*, *P. aeruginosa*, or *C. albicans*. The results indicate that piezoelectric inkjet printing may be useful for loading gauze with both antibacterial and antifungal pharmacologic agents with poor solubility in aqueous solutions for the treatment of mixed wounds.

**Keywords**

inkjet printing, controllable drug doses, amphotericin B, azithromycin.

## Introduction

Most wound infections involve a mixture of aerobic and anaerobic microorganisms [1]. Necrotizing soft tissue infections are associated with a mixture of aerobic and anaerobic microorganisms that are commonly associated with the gut [2]. The US Centers for Disease Control and Prevention recognized *Staphylococcus aureus* and *Pseudomonas aeruginosa* as common organisms in surgical wound infections [3]. *S. aureus*, *P. aeruginosa,* and *Candida* species are also commonly found in burns [4]. A recent study by Alves et al. indicates that *S. aureus* and *P. aeruginosa* act synergistically in chronic wounds, with *S. aureus* facilitating the attachment of *P. aeruginosa* to skin cells and *P. aeruginosa* promoting invasiveness by *S. aureus* [5]. *Candida albicans* has also been shown to co-habit in biofilms with *S. aureus* [6]. Management of mixed wound infections can involve treatment with topical antimicrobial agents that show potency against the wound organisms [1, 7].

Inkjet printing is a non-contact approach technology that may be used to process 1-100 picoliter liquid droplets at a micrometer-scale resolution [8, 9]. In piezoelectric inkjet printing, drops of the ink are ejected from a micrometer-scale nozzle by application of a voltage to a piezoelectric transducer, which generates an acoustic wave and ejects the droplet [9]. Piezoelectric inkjet printing involves the release of droplets from actuation of a piezoelectric transducer. When voltage is applied to a lead zirconate titanate transducer within the printer head, vibrations produce acoustic waves that propel ink through nozzles. The cartridge in the materials deposition system undergoes deformation in what is known as a bender mode, in which transducer actuation takes place in the wafer plane [11]. This approach is associated with low processing costs, generation of minimal waste, and the ability to process pharmaceuticals with minimal contamination [8, 10]. Piezoelectric inkjet printing has been used to process microscale patterns of deoxyribonucleic acid, mussel adhesive protein, streptavidin, and many other types of biological materials [11, 12]. Piezoelectric inkjet printing has also been used to

prepare coatings containing pharmacologic agents on the surfaces of medical devices; for example, a rapamycin derivative antiproliferative agent known as ABT-578 was coated on polymer-coated stainless-steel stents using piezoelectric inkjet printing by Tarcha et al. [13]. They indicated that inkjet printing has the advantage of (a) the reproducible attributes of the droplets in the jet stream and (b) the capability of directing the jet stream to precise regions on the surface of the medical device. Inkjet technology can provide significant improvement in drug loading efficiency comparing with conventional coating methods. Antohe and Wallace coated the antiproliferative agent paclitaxel on drug-eluting stents with piezoelectric inkjet printing [14]. They proposed that the local drug delivery propose could be achieved by piezoelectric inkjet printing. Piezoelectric inkjet printing also has the advantage of coating multiple layers to control the release of one or more drugs depending on the medical status of the patient. Piezoelectric inkjet printing was also used to coat antimicrobial materials including rifampicin and isoniazid on the surfaces of orthopedic implant materials [15, 16]. For example, Gu et al. loaded rifampicin in the micropatterns fabricated by piezoelectric inkjet printing. Their results show that the rate of rifampicin release was strongly influenced by the rifampicin loading in the micropattern. Also, rifampicin containing micropatterns effectively prevented the formation of *Staphylococcus* epidermidis biofilm colonies due to their ability to kill bacteria prior to the formation of colonies on the patterned surfaces [15].

In recent work, we demonstrated piezoelectric inkjet printing of pharmacologic agents with poor solubility in water onto the surfaces of microneedles [17, 18, 19]. For example, we used piezoelectric inkjet printing to deposit amphotericin B on the surfaces of a microneedle array that was made from a biodegradable acid anhydride copolymer [17]. A disk diffusion assay was used to evaluate the antifungal activity of the amphotericin B-loaded microneedles; the amphotericin B-loaded microneedles were shown to possess activity against *Candida parapsilosis*. In another study, piezoelectric inkjet printing was used to deposit coatings of an

imidazole antifungal agent known as miconazole on the surfaces of biodegradable acid anhydride copolymer microneedles; the miconazole-coated microneedles exhibited antifungal activity against *C. albicans* [18]. More recently, we used piezoelectric inkjet printing to deposit an itraconazole-containing solution on the surfaces of solid poly(glycolic acid) microneedles [19]. The surfaces of the microneedles were coated using a two-step process, which included (a) an underlying water-soluble drug release layer containing poly(methyl vinyl ether-co-maleic anhydride) and (b) a surface drug-loaded layer containing itraconazole and coconut oil. A disk diffusion assay showed that the itraconazole-modified microneedle arrays were effective in inhibiting the growth of *C. albicans*.

In this study, we deposited the antifungal agent amphotericin B and the antibacterial agent azithromycin, which exhibit poor solubility in water, on the surfaces of gauze, silicon, and aluminum. 3D laser scanning optical microscopy, Fourier transform infrared spectroscopy, X-ray photoelectron spectroscopy, and an in vitro disk diffusion assay were used to understand the characteristics of the inkjet printing-modified surfaces. The results of this study indicate that piezoelectric inkjet printing may be useful for loading gauze with both antibacterial and antifungal pharmacologic agents for the treatment of mixed wounds.

**Results and Discussion**

The surface morphology of the inkjet printing-modified surfaces on aluminum was evaluated with a confocal laser scanning microscope as shown in Figure 1. The results indicate that the surface morphology of inkjet printing sample was rougher with higher drug loading; roughness data measurements confirmed this trend. The confocal laser scanning microscope roughness data from the inkjet printing-modified surfaces, which was collected using three replicates for each sample type, is shown in Table 1. The roughness data shown in Table 1 include mean and standard deviation values. The term Sa represents the arithmetical mean

roughness, the term Sz represents the peak valley roughness, and the term Sq represents the root mean square roughness. The data showed that the roughness of the pharmacologic agent-modified Al disk was higher than that of the dimethyl sulfoxide-modified Al disk. In addition, the roughness of the Al disk containing a high concentration of the pharmacologic agent was higher than that of the Al disk containing a low concentration of the pharmacologic agent. The results indicate that the surfaces modified with larger amounts of the pharmacologic agent exhibited higher levels of roughness.

The Fourier transform infrared spectra for the dimethyl sulfoxide-modified surface, azithromycin low concentration coating, azithromycin high concentration coating, amphotericin B low concentration coating, amphotericin B high concentration coating, low azithromycin + amphotericin B coating, and high azithromycin + amphotericin B coating are shown in Figure 2. The peaks at 3480, 1726, and 1050 $cm^{-1}$ in the azithromycin-containing coatings are associated with O-H stretching, lactone carbonyl C=O stretching, and asymmetric C-O-C stretching in azithromycin [21, 22]. The contribution of amphotericin B to the spectra is associated with $CH_2$ bending (1250 cm), C–O stretching (around 1380 $cm^{-1}$), COO-stretching (around 1650 $cm^{-1}$), C=O vibrations (around 1720 $cm^{-1}$), C–H stretching (around 3000 $cm^{-1}$), and O–H stretching (around 3350 $cm^{-1}$) [23, 24]. Free −NH stretching vibrations are normally seen at 3300–3500 $cm^{-1}$, while features associated with H bonded N-H appear at 3070–3350 $cm^{-1}$ [25]. The major absorption band at 1050 $cm^{-1}$ is attributed to S-O stretching in dimethyl sulfoxide [26]. The results indicate that the chemical functionality of the inkjet printing-deposited coatings is similar to those of the precursor materials. The spectral features for the inkjet printing-deposited coatings do not show a noticeable departure (indicative of chemical modification) from the precursor materials.

X-ray photoelectron spectra survey scans (in Figure 3) indicated that all of the inkjet printing-modified surfaces contained C, O, Si, which is associated with the dimethyl sulfoxide

solvent, and Al, which is associated with the disk. The azithromycin low concentration coating, azithromycin high concentration coating, amphotericin B high concentration coating, low azithromycin + amphotericin B coating, and high azithromycin + amphotericin B coating also contained N. Figure 4 shows the Carbon 1s X-ray photoelectron spectra of the inkjet printing-modified surfaces on aluminum. Table 2 shows the chemical states of the inkjet printing-modified surfaces on aluminum after curve fitting and peak assignment. The binding energies at 285.0 eV were assigned to C-C bonding, 286.6 eV were assigned to C-O bonding, 287.9 eV were assigned to C=O bonding, and 289.3 eV were assigned to O-C=O bonding. The C1s spectra of the azithromycin low concentration coating and the azithromycin high concentration coating corresponded with that of pure azithromycin [25]. The spectral features in the azithromycin- and amphotericin B-modified surfaces correspond with the bonding of the coating constituents. No unanticipated impurities, including impurities associated with known toxicity, were noted.

The disk diffusion assay from the inkjet printing-modified surfaces as determined using *S. aureus, P. aeruginosa* and *C. albicans* are shown in Figure 5, Figure 6 and Figure 7, respectively. Table 3 shows a summary of the zones of inhibition for the inkjet printing-modified surfaces as determined using the disk diffusion assay. The modified disk diffusion assay result for the dimethyl sulfoxide-coated surfaces (which served as a control) showed no inhibition of *S. aureus*, *P. aeruginosa*, or *C. albicans*. The amphotericin B low concentration coating and the amphotericin B high concentration coating showed 100% inhibition of *C. albicans* in zones that measured 23 mm and 24 mm, respectively (Figure 5). These results are comparable to those from paper disks that were modified with 10 µg of amphotericin B [27]. The azithromycin low concentration coating and the azithromycin high concentration coating showed inhibition of *S. aureus* and *P. aeruginosa*. The results for the inkjet printing-modified

silicon wafers and Al disks showed concentration-dependent antibacterial activity, with coatings containing higher amounts of azithromycin showing higher antibacterial activity. The low azithromycin (Az) + amphotericin B (Amph B) coating and high azithromycin + amphotericin B coating showed concentration-dependent antibacterial activity, with coatings containing higher amounts of azithromycin showing higher antibacterial activity. However, the low azithromycin + amphotericin B coating and high azithromycin + amphotericin B coating did not show concentration-dependent antifungal activity. The absence of potent antifungal activity by the amphotericin B-modified gauze may be attributed to the retention of amphotericin B by the gauze. It is anticipated that the incorporation of an underlying release layer made of poly(methyl vinyl ether-co-maleic anhydride or another water-soluble material may facilitate the development of bandage coatings with stronger antifungal activity [19].

**Conclusions**

Azithromycin and amphotericin B coatings were successfully deposited on the surfaces of gauze, silicon, and aluminum using piezoelectric inkjet printing. 3D laser scanning optical microscopy showed that the surfaces modified with larger amounts of the pharmacologic agent exhibited higher levels of roughness. X-ray photoelectron spectroscopy showed that the inkjet printing-modified surfaces contained the elements and types of bonding associated with the constituent pharmacologic agents or solvent. The Fourier transform infrared spectroscopy results showed the presence of the functional groups associated with the constituent pharmacologic agents and solvent in the coatings. The in vitro disk diffusion assay indicated that the amphotericin B-modified surfaces showed antifungal activity against *C. albicans*; in addition, the azithromycin-modified surfaces showed antibacterial activity against *S. aureus* and *P. aeruginosa*. The incorporation of a release layer containing poly(methyl vinyl ether-co-maleic anhydride or another water-soluble material may enhance the antimicrobial functionality of the coatings. These results indicate the promise of piezoelectric inkjet printing

for loading gauze with both antibacterial and antifungal pharmacologic agents for the treatment of mixed wounds.

## Materials & Methods

### *Materials*

Azithromycin ($C_{38}H_{72}N_2O_{12}$) was purchased from Tocris Bioscience™ (Bristol, United Kingdom). Amphotericin B USP $C_{47}H_{73}NO_{17}$ was purchased from VWR (Radnor, PA, USA). One inch-wide sterile gauze was purchased from Dynarex (Jacksonville, FL, USA); 22 mm x 22 mm wafers were purchased from UniversityWafer (South Boston, MA, USA). The solvent used in this study was ACS reagent grade ( $\geq$ 99.9%) dimethyl sulfoxide ($(CH_3)_2SO$) (DMSO) (MilliporeSigma, St. Louis, MO, USA).

Considering the solubility of azithromycin and amphotericin B in dimethyl sulfoxide, the azithromycin low concentration ink contained 7.5 mg/ml of the pharmacologic agent, the azithromycin high concentration ink contained 75 mg/ml of the pharmacologic agent, the amphotericin B low concentration ink contained 2.5 mg/ml of the pharmacologic agent, and the amphotericin B high concentration ink contained 25 mg/ml of the pharmacologic agent.

### *Inkjet printer*

Deposition of the amphotericin B and azithromycin coatings were performed using a Dimatix DMP-2831 material printer (Fujifilm Dimatix, Santa Clara, CA, USA) and a DMCLCP-11610 inkjet cartridge (Fujifilm Dimatix, Santa Clara, CA, USA). The inkjet cartridges were loaded with at least 1.0 mL of solution using a syringe and a blunt-tipped needle; these cartridges were used to eject droplets with nominal volumes of 10 pL per droplet. A separate cartridge was used for each type of ink.

### *Coating of the aluminum disks*

The printed surfaces were made up of an array of "dots." The aluminum disks were coated with an array pattern containing 21 dots by 21 dots. The azithromycin low concentration

coating contained 30 layers of droplets; based on the number of droplets and the ink concentration, 24.81 µg of azithromycin was deposited. The azithromycin high concentration coating contained 30 layers of droplets; based on the number of droplets and the ink concentration, 248.06 µg of azithromycin was deposited. The amphotericin B low concentration coating contained 30 layers of droplets; based on the number of droplets and the ink concentration, 8.27 µg of amphotericin B was deposited. The amphotericin B high concentration coating contained 30 layers of droplets; based on the number of droplets and the ink concentration, 82.69 µg of amphotericin B was deposited.

The low azithromycin + amphotericin B coating contained 30 layers of droplets, including 15 layers of the azithromycin low concentration ink and 15 layers of the amphotericin B low concentration ink. Based on the number of droplets and the ink concentration, 12.40 µg of azithromycin and 4.13 µg of amphotericin B were deposited. The high azithromycin + amphotericin B coating contained 30 layers of droplets, including 15 layers of the azithromycin high concentration ink and 15 layers of the amphotericin B high concentration ink. Based on the number of droplets and the ink concentration, 124.03 µg of azithromycin and 41.34 µg of amphotericin B were deposited.

*Coating of the silicon wafers*

The silicon wafers were coated with an array pattern containing 21 dots by 21 dots. The azithromycin low concentration coating contained 30 layers of droplets; based on the number of droplets and the ink concentration, 24.81 µg of azithromycin was deposited. The azithromycin high concentration coating contained 30 layers of droplets; based on the number of droplets and the ink concentration, 248.06 µg of azithromycin was deposited. The amphotericin B low concentration coating contained 30 layers of droplets; based on the number of droplets and the ink concentration, 8.27 µg of amphotericin B was deposited. The

amphotericin B high concentration coating contained 30 layers of droplets; based on the number of droplets and the ink concentration, 82.69 µg of amphotericin B was deposited.

The low azithromycin + amphotericin B coating contained 30 layers of droplets, including 15 layers of the azithromycin low concentration ink and 15 layers of the amphotericin B low concentration ink. Based on the number of droplets and the ink concentration, 12.40 µg of azithromycin and 4.13 µg of amphotericin B were deposited. The high azithromycin + amphotericin B coating contained 30 layers of droplets, including 15 layers of the azithromycin high concentration ink and 15 layers of the amphotericin B high concentration ink. Based on the number of droplets and the ink concentration, 124.035 µg of azithromycin and 41.34 µg of amphotericin B were deposited.

*Coating of the gauze pieces*

The gauze pieces were coated with an array pattern containing 84 dots by 21 dots. The azithromycin low concentration coating contained 30 layers of droplets; based on the number of droplets and the ink concentration, 99.23 µg of azithromycin was deposited. The azithromycin high concentration coating contained 30 layers of droplets; based on the number of droplets and the ink concentration, 992.25 µg of azithromycin was deposited. The amphotericin B low concentration coating contained 30 layers of droplets; based on the number of droplets and the ink concentration, 33.075 µg of amphotericin B was deposited. The amphotericin B high concentration coating contained 30 layers of droplets; based on the number of droplets and the ink concentration, 330.75 µg of amphotericin B was deposited.

The low azithromycin + amphotericin B coating contained 30 layers of droplets, including 15 layers of the azithromycin low concentration ink and 15 layers of the amphotericin B low concentration ink. Based on the number of droplets and the ink concentration, 49.61 µg of azithromycin and 16.54 µg of amphotericin B were deposited. The high azithromycin + amphotericin B coating contained 30 layers of droplets, including 15 layers of the azithromycin

high concentration ink and 15 layers of the amphotericin B high concentration ink. Based on the number of droplets and the ink concentration, 496.13 μg of azithromycin and 165.38 μg of amphotericin B were deposited.

*Materials characterization*

The roughness of the inkjet printing-modified surfaces was quantified using a VKx1100 confocal laser scanning microscope (Keyence, Osaka, Japan). The roughness was measured at the center of the inkjet printing-modified region on the aluminum (Al) disks. A SPECS System with PHOIBOS 150 Analyzer (SPECS Surface Nano Analysis GmbH, Berlin, Germany) was used to obtain X-ray photoelectron spectroscopy data from the inkjet printing-modified Al disks. Fourier transform infrared spectroscopy (FTIR) data were obtained from the inkjet printing-modified Al disks using a Nexus 470 system with an OMNI sampler, a continuum microscope, and OMNIC$^{TM}$ analysis software (Thermo Fisher, Waltham, MA, USA). The spectra were collected over a wavenumber range of 500- 4000 $cm^{-1}$ with a resolution of 2 $cm^{-1}$ at room temperature. Each sample was analysed in triplicate; the average was compared.

*Antimicrobial testing*

Antimicrobial testing of the inkjet printing-modified surfaces was performed as described previously [20]. Luria-Bertani broth, tryptic soy broth, Mueller Hinton agar, yeast nitrogen base, Sabouraud dextrose agar, dextrose, agar, and phosphate-buffered saline (x 10) were obtained from VWR (Radnor, PA, USA). Phosphate buffered saline (PBS) (x 1) was made by dilution in deionized water. The microorganisms utilized in the study were acquired from American Type Culture Collection (Manassas, VA, USA); the microorganisms included *Candida albicans* ATCC 90028, *Pseudomonas aeruginosa* ATCC 15442, and *Staphylococcus aureus* ATCC 6538. Cultures were prepared overnight with *P. aeruginosa* in tryptic soy broth, *S. aureus* in tryptic soy broth, and *C. albicans* in yeast nitrogen base and 100 mM dextrose.

The cultures were pelleted by centrifugation at 4500 rpm for 10 minutes and resuspended in PBS (x 1) to a cell density of ~$10^8$ cells $mL^{-1}$. Sterile swabs were used to inoculate the agar plates with the lawns of the microorganisms. *C. albicans* lawns were inoculated on Sabouraud dextrose agar plates. The *P. aeruginosa* and *S. aureus* lawns were inoculated on Mueller Hinton agar plates containing the respiratory indicator dye, triphenyltetrazolium chloride (70 mg/l *P. aeruginosa*; 50 mg/L *S. aureus*) to facilitate visualization of microbial growth (i.e., red colorization). The dimethyl sulfoxide-modified surfaces and pharmacologic agent-modified surfaces were examined for antimicrobial activity using the modified-disk diffusion agar plating assay. The dimethyl sulfoxide-modified surfaces and pharmacologic agent-modified surfaces were applied to the inoculated agar plates and incubated for 24 h at 37˚C. Inhibition of growth on the plates was evaluated using digital images that were obtained following 24 h of incubation.

*Statistical analysis*

Statistical analysis was conducted using Excel software (Microsoft Corporation, Albuquerque, NM, USA). All the quantitative data were expressed as the average ± standard deviation of the mean.

**Acknowledgments**

The authors (S. J. S. and L. V.) would like to acknowledge support from the Office of Naval Research (N00014-20-1-2236).

**Conflict of interest statement**

On behalf of all authors, the corresponding author states that there is no conflict of interest.

**Data availability**

The datasets generated during and/or analyzed during the current study are available from the corresponding author on reasonable request.

**References**

1. P. G. Bowler, B. I. Duerden, D. G. Armstrong, Clin. Microbiol. Rev. 14, 244 (2001).

2. D. Kingston, D. V. Seal, Br. J. Surg. 77, 260 (1990).

3. A. J. Mangram, T. C. Horan, M. L. Pearson, L. C. Silver, W. R. Jarvis, Infect. Control Hosp. Epidemiol. 20, 247 (1999).

4. P. G. Bowler, B. I. Duerden, D. G. Armstrong, Clin. Microbiol. Rev. 14, 244 (2001).

5. P. M. Alves, E. Al-Badi, C. Withycombe, P. M. Jones, K. J. Purdy, S. E. Maddocks, Pathog. Dis. 76, 003 (2018).

6. R. U. Pathirana, A. D. McCall, H. L. Norris, M. Edgerton, Front. Microbiol. 10, 1188 (2019).

7. B. G. MacMillan, Surg. Clin. North Am. 60, 185 (1980).

8. J. T. Delaney, P. J. Smith, U. S. Schubert, Soft Matter 5, 4866 (2009).

9. B. Derby, Ann. Rev. Mater. Sci. 40, 395 (2010).

10. P. W. Cooley, D. B. Wallace, B. V. Antohe, Proc. SPIE Conf. Microfluidics, BioMEMS, Med. Microsyst. 177 (2001).

11. J. Sumerel, J. Lewis, A. Doraiswamy, L. F. Deravi, S. L. Sewell, A. E. Gerdon, D. W. Wright, R. J. Narayan, Biotechnol. J. 1, 976 (2006).

12. A. Doraiswamy, T. M. Dunaway, J. J. Wilker, R. J. Narayan, J. Biomed. Mater. Res. 89B, 28 (2009).

13. P. J. Tarcha, D. Verlee, H. W. Hui, J. Setesak, B. Antohe, D. Radulescu, D. Wallace, Ann. Biomed. Eng. 35, 1791 (2007).

14. B. V. Antohe, D. B. Wallace, Int. Manufact. Sci. Eng. Conf. 48524, 525 (2008).

15. Y. Gu, X. Chen, J. H. Lee, D. A. Monteiro, H. Wang, W. Y. Lee, Acta Biomater. 8, 424 (2012).

16. Wu W, Zheng Q, Guo X, Sun J, Liu Y. Biomedical Materials. 2009 Nov 9;4(6):065005.

17. R. D. Boehm, P. R. Miller, W. A. Schell, J. R. Perfect, R. J. Narayan, JOM. 65, 525 (2013).

18. R. D. Boehm, P. R. Miller, J. Daniels, S. Stafslien, R. J. Narayan, Mater. Today 17, 247 (2014).

19. R. D. Boehm, J. Daniels, S. Stafslien, A. Nasir, J. Lefebvre, R. J. Narayan, Biointerphases 10, 011004 (2015).

20. R. J. Narayan, S. P. Adiga, M. J. Pellin, L. A. Curtiss, S. Stafslien, B. Chisholm, N. A. Monteiro-Riviere, R. L. Brigmon, J. W. Elam, Mater. Today 13, 60 (2010).

21. N. F. Robaina, C. E. de Paula, D. M. Brum, M. de la Guardia, S. Garrigues, R. J. Cassella, Microchem. J. 110, 301 (2013).

22. S. Mangal, R. Xu, H. Park, D. Zemlyanov, N. Shetty, Y. W. Lin, D. Morton, H. K. Chan, J. Li, Q. T. Zhou, Pharm. Res. 36, 6 (2019).

23. P. K. Singh, P. Sah, J. G. Meher, S. Joshi, V. K. Pawar, K. Raval, Y. Singh, K. Sharma, A. Kumar, A. Dube, M. K. Chourasia, RSC Adv. 6, 71705 (2016).

24. M. Gagoś, M. Arczewska, Europ. Biophys. J. 41, 663 (2012).

25. G.C. Silva, C.B. Yeamans, P.F. Weck, J.D. Hunn, G.S. Cerefice, A.P. Sattelberger, K.R. Czerwinski, Synthesis and Characterization of Th2N2 (NH) Isomorphous to Th2N3, Inorganic chemistry 51(5), 3332-3340 (2012).

26. V. M. Wallace, N. R. Dhumal, F. M. Zehentbauer, H. J. Kim, J. Kiefer, J. Phys. Chem. B 119, 14780 (2015).

27. Q. T. Zhou, Z. H. Loh, J. Yu, S. P. Sun, T. Gengenbach, J. A. Denman, J. Li, H. K. Chan, AAPS J. 18, 1213 (2016).

28. A. Espinel-Ingroff, E. Canton, A. Fothergill, M. Ghannoum, E. Johnson, R. N. Jones, L. Ostrosky-Zeichner, W. Schell, D. L. Gibbs, A. Wang, J. Turnidge, J. Clin. Microbiol. 49, 2568 (2011).

**Figures and Table Captions.**

Table 1. Roughness parameters for the inkjet printing-modified surfaces on aluminum as determined using 3D laser scanning microscopy.

Table 2. Chemical states of the inkjet printing-modified surfaces on aluminum as determined using X-ray photoelectron spectroscopy.

Table 3. Zones of inhibition for the inkjet printing-modified surfaces as determined using the disk diffusion assay. "-" and "+" indicate the absence or presence of a zone of inhibition, respectively.

Figure 1. Surface morphology of the inkjet printing-modified surfaces on aluminum measured via confocal laser scanning microscope: (a) dimethyl sulfoxide-modified surface, (b) azithromycin low concentration coating, (c) azithromycin high concentration coating, (d) amphotericin B low concentration coating, (e) amphotericin B high concentration coating, (f) low azithromycin + amphotericin B coating, and (g) high azithromycin + amphotericin B coating. The scale bar represents 50 μm.

Figure 2. Fourier transform infrared spectra from the inkjet printing-modified surfaces on aluminum: (a) dimethyl sulfoxide-modified surface, (b) azithromycin low concentration coating, (c) azithromycin high concentration coating, (d) amphotericin B low concentration coating, (e) amphotericin B high concentration coating, (f) low azithromycin + amphotericin B coating, and (g) high azithromycin + amphotericin B coating.

Figure 3. XPS survey spectrum from the inkjet printing-modified surfaces on aluminum: (a) dimethyl sulfoxide-modified surface, (b) azithromycin low concentration coating, (c) azithromycin high concentration coating, (d) amphotericin B low concentration coating, (e) amphotericin B high concentration coating, (f) low azithromycin + amphotericin B coating, and (g) high azithromycin + amphotericin B coating.

Figure 4. Carbon 1s X-ray photoelectron spectra from the inkjet printing-modified surfaces on aluminum: (a) dimethyl sulfoxide-modified surface, (b) azithromycin low concentration coating, (c) azithromycin high concentration coating, (d) amphotericin B low concentration coating, (e) amphotericin B high concentration coating, (f) low azithromycin + amphotericin B coating, and (g) high azithromycin + amphotericin B coating.

Figure 5. Disk diffusion assay from the inkjet printing-modified surfaces as determined using *Staphylococcus aureus*.

Figure 6. Disk diffusion assay from the inkjet printing-modified surfaces as determined using *Pseudomonas aeruginosa*. Please note that the silicon wafers migrated across the MH agar toward the edge of the Petri dish during the 24 incubation period, but did not compromise the discernment and quantitation of zones of growth inhibition.

Figure 7. Disk diffusion assay from the inkjet printing-modified surfaces as determined using *Candida albicans*.

Table 1.

| | **Roughness parameters** | | |
|---|---|---|---|
| Sample | Sa μm | Sz μm | Sq μm |
| DMSO | 0.35±0.04 | 6.04±2.32 | 0.44±0.05 |
| low azithromycin | 0.40±0.06 | 7.94±5.00 | 0.58±0.14 |
| high azithromycin | 1.37±0.45 | 15.66±3.35 | 1.89±0.55 |
| low amphotericin B | 0.46±0.06 | 4.89±2.00 | 0.60±0.12 |
| high amphotericin B | 2.11±2.70 | 18.32±19.83 | 3.09±4.16 |
| low azithromycin + amphotericin B | 3.34±1.54 | 24.38±9.49 | 4.64±2.41 |
| high azithromycin + amphotericin B | 3.65±1.24 | 24.39±4.68 | 4.52±1.18 |

Table 2.

| | Percent of chemical states | | | |
|---|---|---|---|---|
| Sample | C-C | C-O | C=O | O-C=O |
| DMSO | 76.2 | 16.3 | 0.3 | 7.2 |
| low azithromycin | 58.6 | 33.4 | 4.3 | 3.6 |
| high azithromycin | 69.8 | 23.9 | 4.8 | 1.6 |
| low amphotericin B | 69.5 | 20.5 | 5.2 | 4.9 |
| high amphotericin B | 68.0 | 20.8 | 7.2 | 4.0 |
| low azithromycin + amphotericin B | 62.3 | 28.6 | 7.0 | 2.1 |
| high azithromycin + amphotericin B | 57.1 | 33.8 | 5.5 | 3.7 |

Table 3.

| | **Disk diffusion assay zone of inhibition (mm)** | | |
|---|---|---|---|
| Sample | S. aureus | P. aeruginosa | C. albicans |
| DMSO on Al disk | 0 | 0 | 0 |
| DMSO on Si wafer | 0 | 0 | 0 |
| DMSO on gauze piece | "-" | "-" | "-" |
| low azithromycin on Al disk | 29 | 27 | 0 |
| low azithromycin on Si wafer | 31 | 26 | 0 |
| low azithromycin on gauze piece | "+" | "+" | "-" |
| high azithromycin on Al disk | 38 | 38 | 0 |
| high azithromycin on Si wafer | 37 | 37 | 0 |
| high azithromycin on gauze piece | "+" | "+" | "-" |
| low amphotericin B on Al disk | 0 | 0 | 0 |
| low amphotericin B on Si wafer | 0 | 0 | 23 |
| low amphotericin B on gauze piece | "-" | "-" | "-" |
| high amphotericin B on Al disk | 0 | 0 | 21 |
| high amphotericin B on Si wafer | 0 | 0 | 24 |
| high amphotericin B on gauze piece | "-" | "-" | "-" |
| low azithromycin + amphotericin B on Al disk | 26 | 0 | 18 |
| low azithromycin + amphotericin B on Si wafer | 21 | 0 | 22 |
| low azithromycin + amphotericin B on gauze piece | "+" | "-" | "-" |
| high azithromycin + amphotericin B on Al disk | 32 | 36 | 22 |
| high azithromycin + amphotericin B on Si wafer | 38 | 32 | 30 |
| high azithromycin + amphotericin B on gauze piece | "+" | "+" | "-" |

**(a) DMSO**

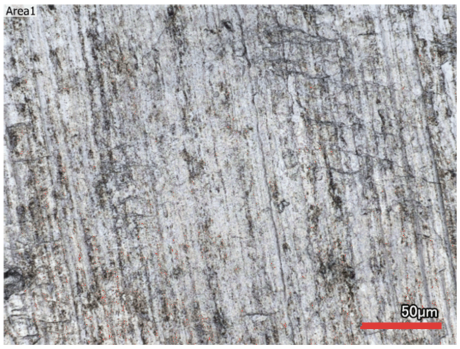


**(b) Low Azithromycin**

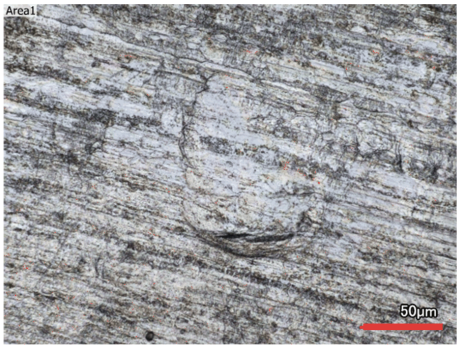


**(c) High Azithromycin**

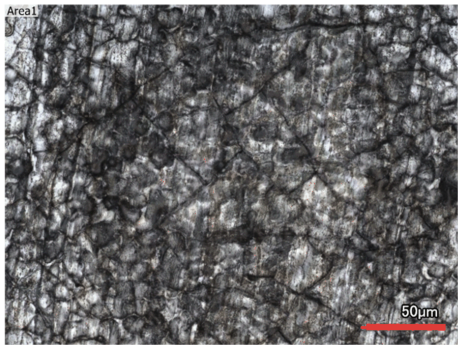


**(d) Low Amphotericin B**

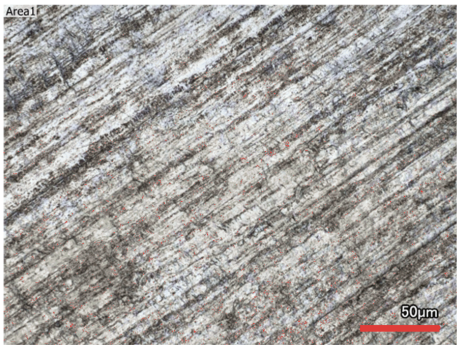


**(e) High Amphotericin B**

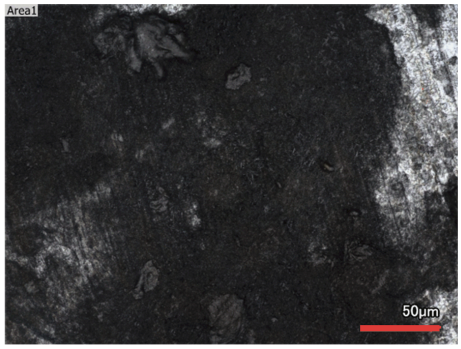


**(f) Low Az + Low Amph B**

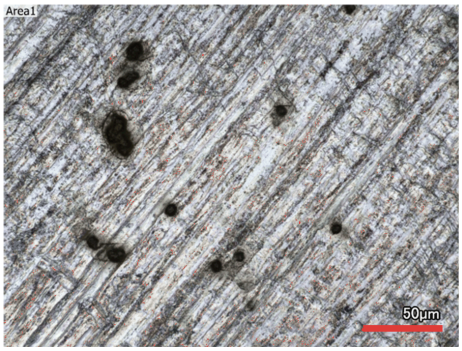


**(g) High Az + Low Amph B**

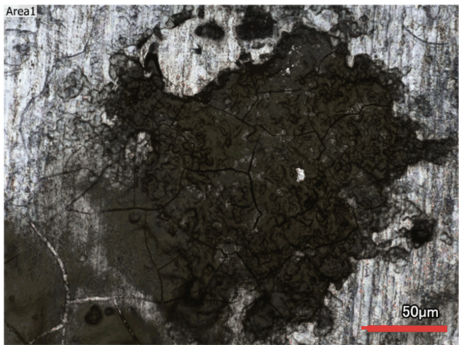


Figure 1.

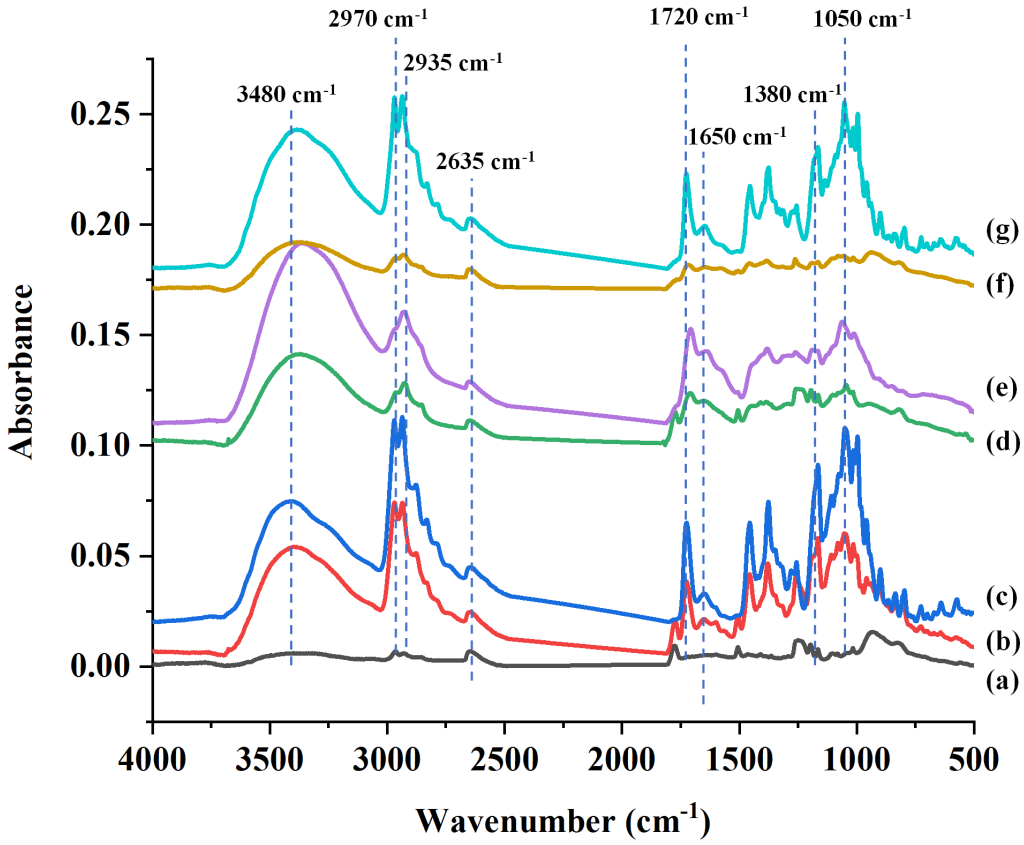
2970 cm-1
2935 cm-1
3480 cm-1
2635 cm-1
1720 cm-1
1050 cm-1
1380 cm-1
1650 cm-1
(g)
(f)
(e)
(d)
(c)
(b)
(a)
Absorbance
0.25
0.20
0.15
0.10
0.05
0.00
4000
3500
3000
2500
2000
1500
1000
500
Wavenumber (cm-1)

Figure 2.

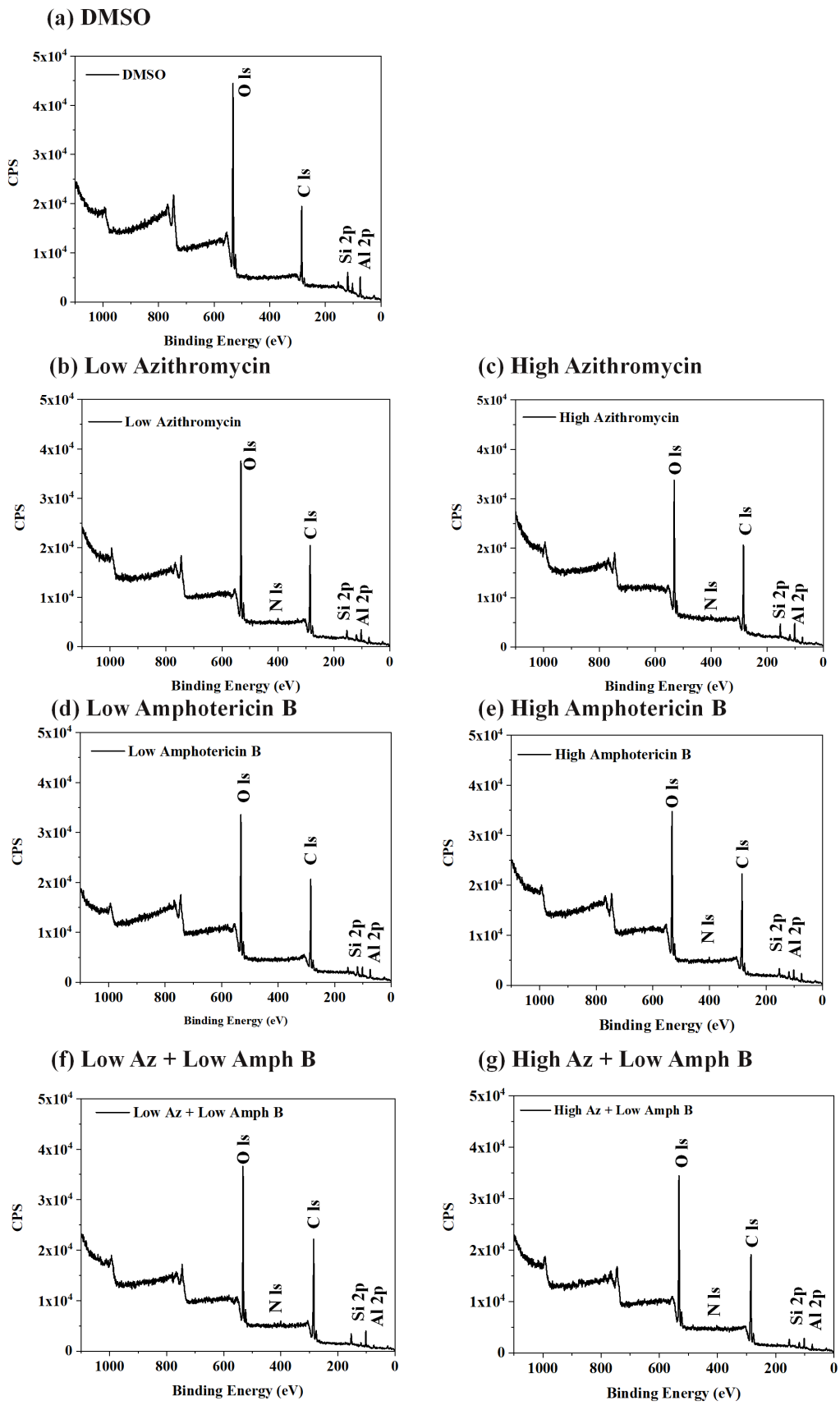
(a) DMSO
DMSO
O 1s
C 1s
Si 2p
Al 2p
CPS
Binding Energy (eV)
(b) Low Azithromycin
Low Azithromycin
O 1s
N 1s
C 1s
Si 2p
Al 2p
CPS
Binding Energy (eV)
(c) High Azithromycin
High Azithromycin
O 1s
N 1s
C 1s
Si 2p
Al 2p
CPS
Binding Energy (eV)
(d) Low Amphotericin B
Low Amphotericin B
O 1s
C 1s
Si 2p
Al 2p
CPS
Binding Energy (eV)
(e) High Amphotericin B
High Amphotericin B
O 1s
N 1s
C 1s
Si 2p
Al 2p
CPS
Binding Energy (eV)
(f) Low Az + Low Amph B
Low Az + Low Amph B
O 1s
N 1s
C 1s
Si 2p
Al 2p
CPS
Binding Energy (eV)
(g) High Az + Low Amph B
High Az + Low Amph B
O 1s
N 1s
C 1s
Si 2p
Al 2p
CPS
Binding Energy (eV)

Figure 3

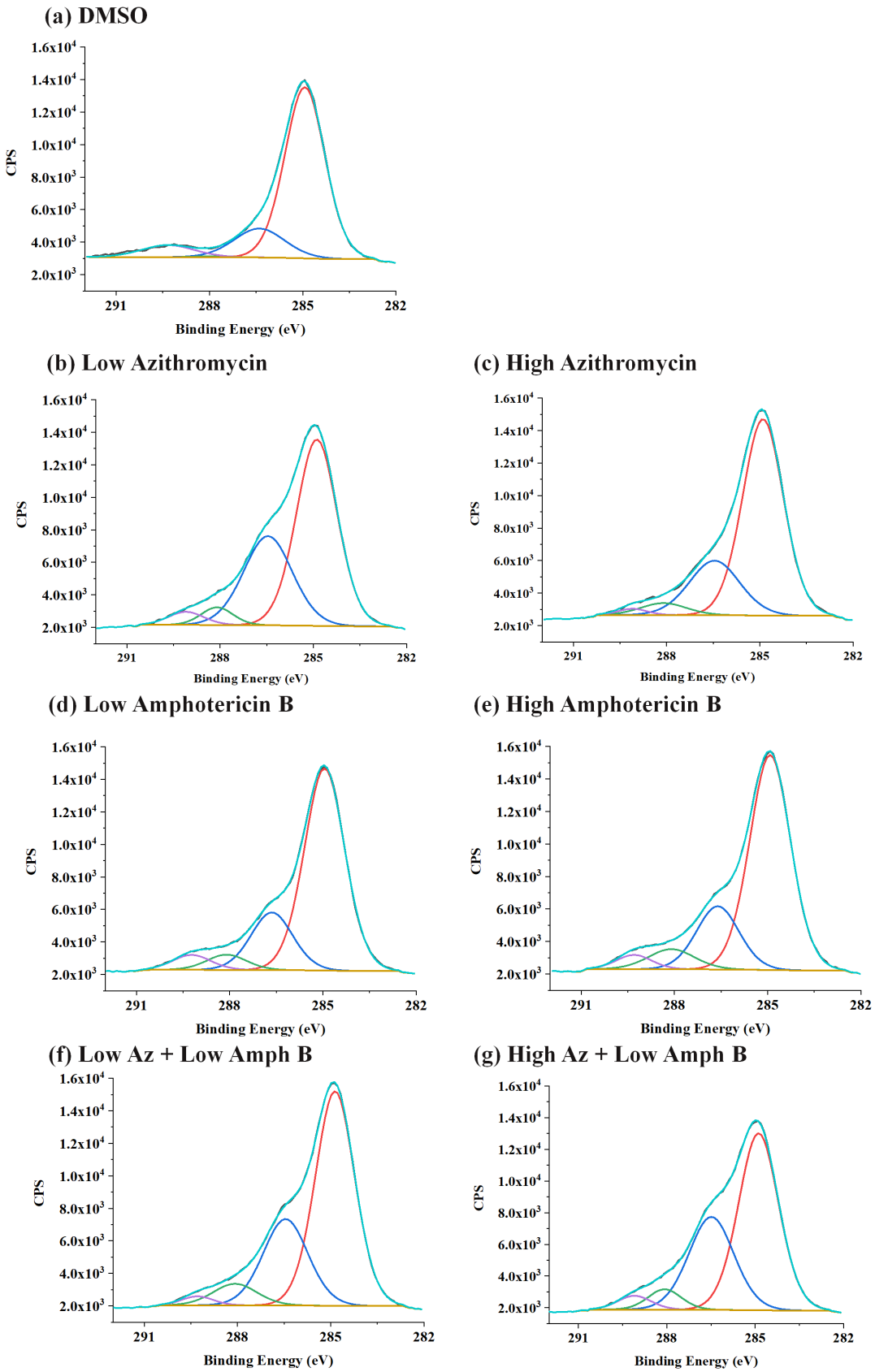
(a) DMSO
(b) Low Azithromycin
(c) High Azithromycin
(d) Low Amphotericin B
(e) High Amphotericin B
(f) Low Az + Low Amph B
(g) High Az + Low Amph B
CPS
Binding Energy (eV)
1.6x10^4
1.4x10^4
1.2x10^4
1.0x10^4
8.0x10^3
6.0x10^3
4.0x10^3
2.0x10^3
291
288
285
282

Figure 4.

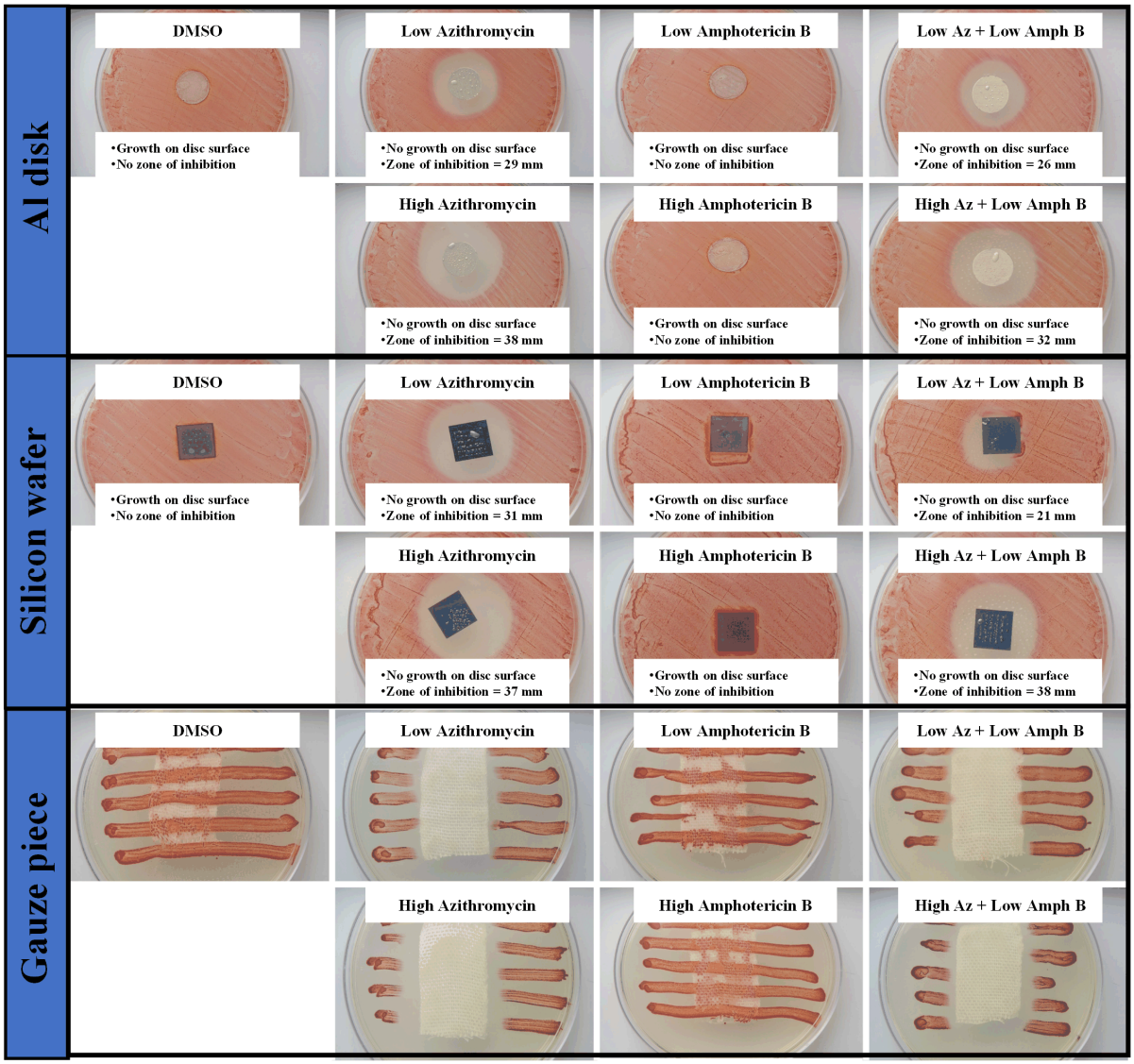
Al disk
Silicon wafer
Gauze piece
DMSO
•Growth on disc surface
•No zone of inhibition
Low Azithromycin
•No growth on disc surface
•Zone of inhibition = 29 mm
Low Amphotericin B
•Growth on disc surface
•No zone of inhibition
Low Az + Low Amph B
•No growth on disc surface
•Zone of inhibition = 26 mm
High Azithromycin
•No growth on disc surface
•Zone of inhibition = 38 mm
High Amphotericin B
•Growth on disc surface
•No zone of inhibition
High Az + Low Amph B
•No growth on disc surface
•Zone of inhibition = 32 mm
DMSO
•Growth on disc surface
•No zone of inhibition
Low Azithromycin
•No growth on disc surface
•Zone of inhibition = 31 mm
Low Amphotericin B
•Growth on disc surface
•No zone of inhibition
Low Az + Low Amph B
•No growth on disc surface
•Zone of inhibition = 21 mm
High Azithromycin
•No growth on disc surface
•Zone of inhibition = 37 mm
High Amphotericin B
•Growth on disc surface
•No zone of inhibition
High Az + Low Amph B
•No growth on disc surface
•Zone of inhibition = 38 mm
DMSO
Low Azithromycin
Low Amphotericin B
Low Az + Low Amph B
High Azithromycin
High Amphotericin B
High Az + Low Amph B

Figure 5.

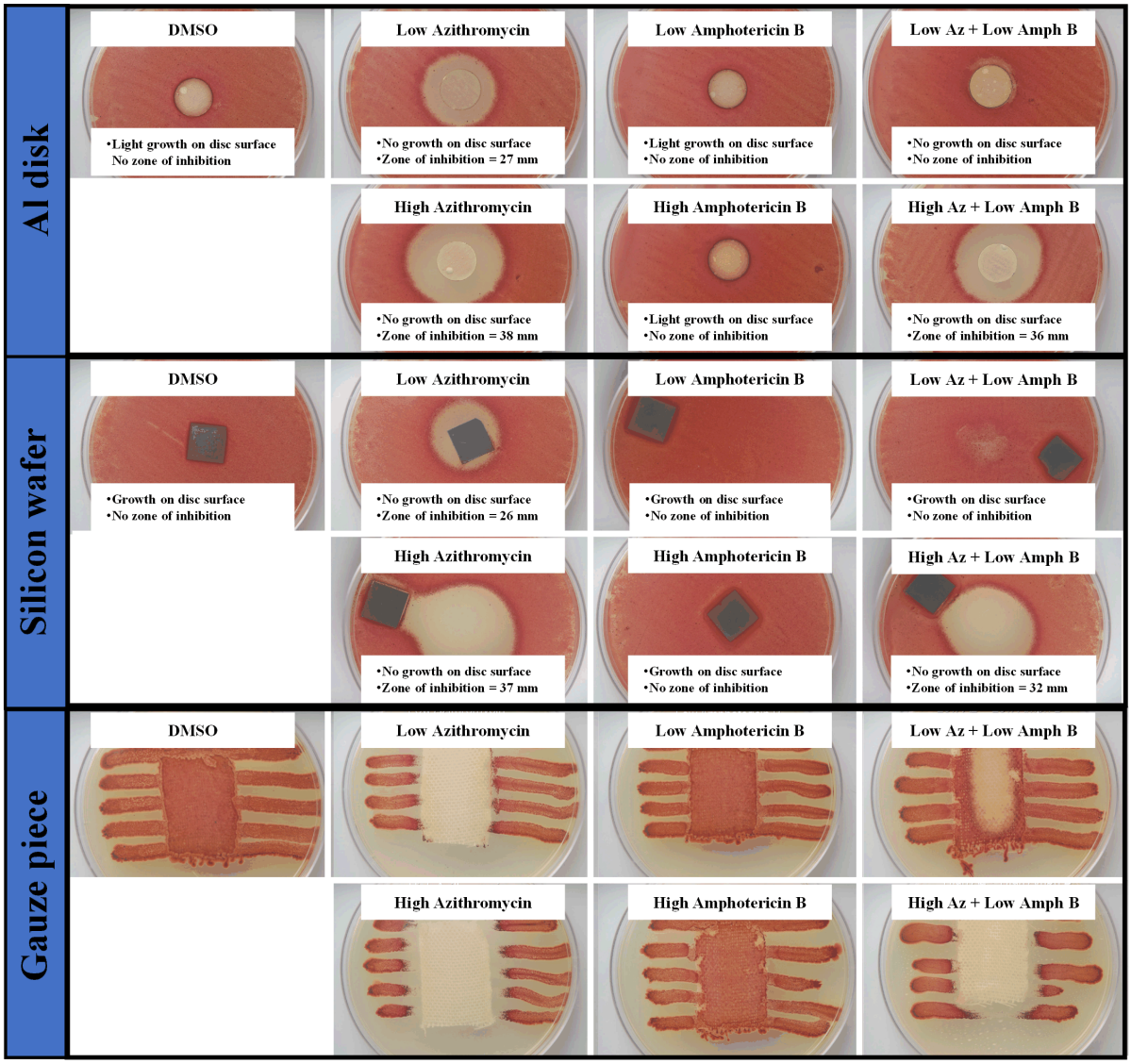
Al disk
Silicon wafer
Gauze piece
DMSO
•Light growth on disc surface
No zone of inhibition
Low Azithromycin
•No growth on disc surface
•Zone of inhibition = 27 mm
Low Amphotericin B
•Light growth on disc surface
•No zone of inhibition
Low Az + Low Amph B
•No growth on disc surface
•No zone of inhibition
High Azithromycin
•No growth on disc surface
•Zone of inhibition = 38 mm
High Amphotericin B
•Light growth on disc surface
•No zone of inhibition
High Az + Low Amph B
•No growth on disc surface
•Zone of inhibition = 36 mm
DMSO
•Growth on disc surface
•No zone of inhibition
Low Azithromycin
•No growth on disc surface
•Zone of inhibition = 26 mm
Low Amphotericin B
•Growth on disc surface
•No zone of inhibition
Low Az + Low Amph B
•Growth on disc surface
•No zone of inhibition
High Azithromycin
•No growth on disc surface
•Zone of inhibition = 37 mm
High Amphotericin B
•Growth on disc surface
•No zone of inhibition
High Az + Low Amph B
•No growth on disc surface
•Zone of inhibition = 32 mm
DMSO
Low Azithromycin
Low Amphotericin B
Low Az + Low Amph B
High Azithromycin
High Amphotericin B
High Az + Low Amph B

Figure 6.

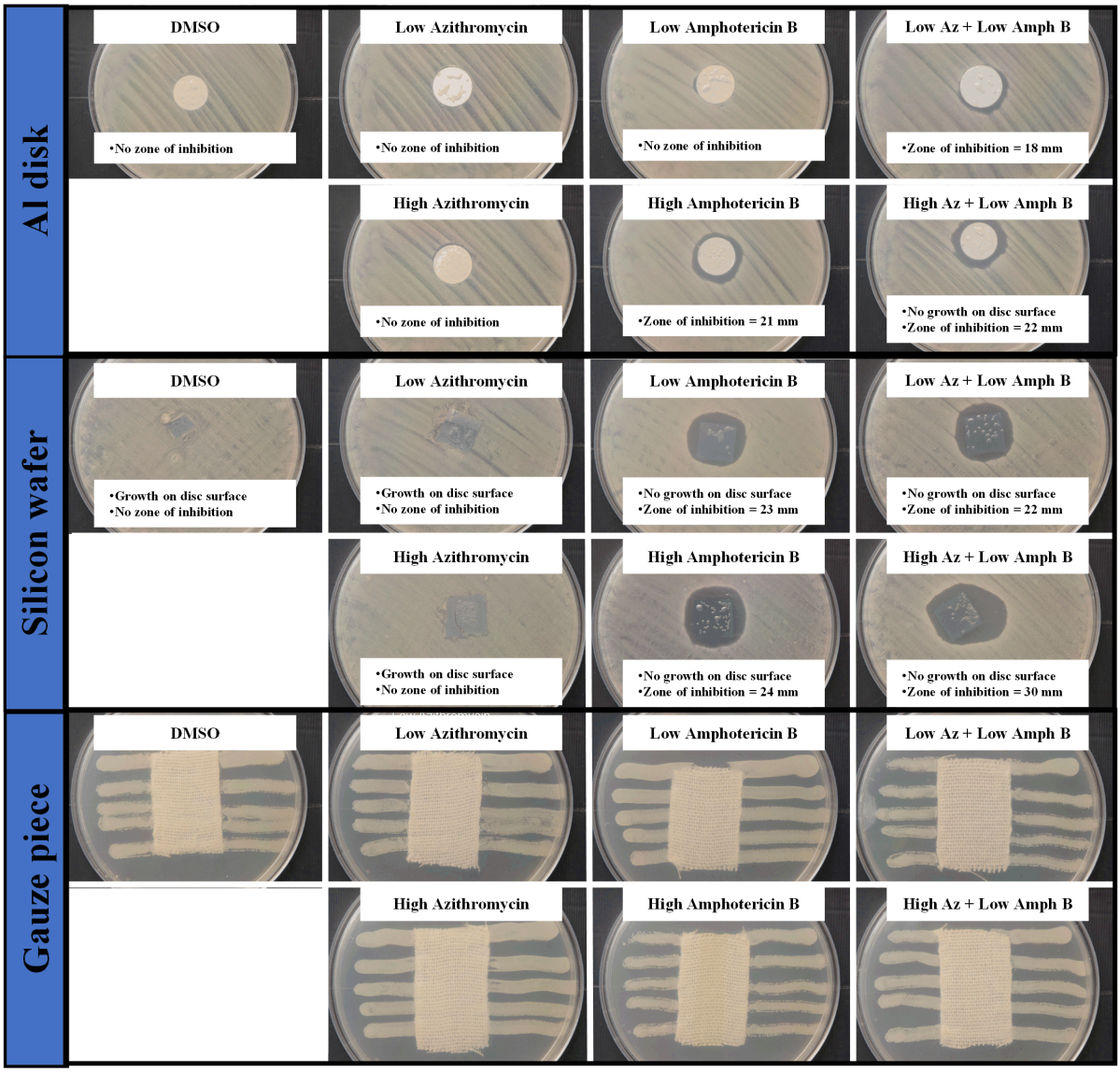
Al disk
Silicon wafer
Gauze piece
DMSO
•No zone of inhibition
Low Azithromycin
•No zone of inhibition
Low Amphotericin B
•No zone of inhibition
Low Az + Low Amph B
•Zone of inhibition = 18 mm
High Azithromycin
•No zone of inhibition
High Amphotericin B
•Zone of inhibition = 21 mm
High Az + Low Amph B
•No growth on disc surface
•Zone of inhibition = 22 mm
DMSO
•Growth on disc surface
•No zone of inhibition
Low Azithromycin
•Growth on disc surface
•No zone of inhibition
Low Amphotericin B
•No growth on disc surface
•Zone of inhibition = 23 mm
Low Az + Low Amph B
•No growth on disc surface
•Zone of inhibition = 22 mm
High Azithromycin
•Growth on disc surface
•No zone of inhibition
High Amphotericin B
•No growth on disc surface
•Zone of inhibition = 24 mm
High Az + Low Amph B
•No growth on disc surface
•Zone of inhibition = 30 mm
DMSO
Low Azithromycin
Low Amphotericin B
Low Az + Low Amph B
High Azithromycin
High Amphotericin B
High Az + Low Amph B

Figure 7.